

Thinking Small: Progress on Microscale Neurostimulation Technology

Joseph J. Pancrazio, PhD*; Felix Deku, MS*; Atefeh Ghazavi, MS*;
Allison M. Stiller, BS*; Rashed Rihani, BS*; Christopher L. Frewin, PhD*;
Victor D. Varner, PhD*; Timothy J. Gardner, PhD[†]; Stuart F. Cogan, ScD*

Objectives: Neural stimulation is well-accepted as an effective therapy for a wide range of neurological disorders. While the scale of clinical devices is relatively large, translational, and pilot clinical applications are underway for microelectrode-based systems. Microelectrodes have the advantage of stimulating a relatively small tissue volume which may improve selectivity of therapeutic stimuli. Current microelectrode technology is associated with chronic tissue response which limits utility of these devices for neural recording and stimulation. One approach for addressing the tissue response problem may be to reduce physical dimensions of the device. "Thinking small" is a trend for the electronics industry, and for implantable neural interfaces, the result may be a device that can evade the foreign body response.

Materials and Methods: This review paper surveys our current understanding pertaining to the relationship between implant size and tissue response and the state-of-the-art in ultrasmall microelectrodes. A comprehensive literature search was performed using PubMed, Web of Science (Clarivate Analytics), and Google Scholar.

Results: The literature review shows recent efforts to create microelectrodes that are extremely thin appear to reduce or even eliminate the chronic tissue response. With high charge capacity coatings, ultramicroelectrodes fabricated from emerging polymers, and amorphous silicon carbide appear promising for neurostimulation applications.

Conclusion: We envision the emergence of robust and manufacturable ultramicroelectrodes that leverage advanced materials where the small cross-sectional geometry enables compliance within tissue. Nevertheless, future testing under *in vivo* conditions is particularly important for assessing the stability of thin film devices under chronic stimulation.

Keywords: Coating, deep brain stimulation, electrodes, microelectrode, neural interface, neurostimulation, stimulation

Conflict of Interest: The authors have no relevant conflicts of interest to disclose.

INTRODUCTION

Neural stimulation is well-accepted as an effective therapy for a wide range of neurological disorders. Deep brain stimulation significantly reduces motor symptoms associated with movement disorders such as essential tremor (1,2) and Parkinson's disease (3,4), and has shown promising results in a range of other disorders (5–7). Driven by one or more implantable pulse generators, DBS electrodes consist of four cylindrical platinum/iridium contacts on the order of 1.27 mm in diameter and often operate as voltage-controlled devices to deliver amplitudes from 1–3 V to stimulate estimated volumes from 100 to 250 mm² of tissue for therapeutic ends (8). Assuming an electrode impedance of 1000–2000 Ω, stimulation currents on the order of 1–3 mA per pulse can result (8). Recent developments have shown the feasibility of horizontal current steering with the use of segmented electrodes (9,10).

While the scale of clinical devices is relatively large, translational, and pilot clinical applications are underway for microelectrode-based systems. Microelectrodes have the advantage of stimulating a relatively small tissue volume which may improve selectivity of therapeutic stimuli (11). Arrays of microelectrodes, which are capable of recording neural signals and microstimulation, are shown in Figure 1. In principal, all electrodes are fundamentally capable of either

recording or stimulation. What limits the utility of microelectrodes for stimulation is whether or not the electrode–electrolyte interface exhibits sufficient charge injection capacity to induce excitation without surpassing safe levels, and the extent that the material is chemically and physically stable with pulsing *in vivo*. The Utah (or Blackrock) devices consist of multiple shanks of length 0.5–1.5 mm and cross-sectional area of 1500–3500 μm² decreasing in dimension approaching the conical tip which consists of either a platinum or

Address correspondence to: Joseph J. Pancrazio, PhD, Department of Bioengineering, The University of Texas at Dallas, 800 W. Campbell Road, BSB 13.633, Richardson, TX 75080, USA. Email: joseph.pancrazio@utdallas.edu

* Department of Bioengineering, The University of Texas at Dallas, Richardson, TX, USA; and

[†] Department of Biology, Boston University, Boston, MA, USA

For more information on author guidelines, an explanation of our peer review process, and conflict of interest informed consent policies, please go to <http://www.wiley.com/WileyCDA/Section/id-301854.html>

Source(s) of financial support: This work was sponsored by the Defense Advanced Research Projects Agency (DARPA) BTO under the auspices of Dr. Douglas Weber through the Space and Naval Warfare Systems Center, Pacific Grant/Contract No. HR0011-15-2-0017 to SFC and a NIH grant U01NS090454-01 to Dr. Timothy Gardner.

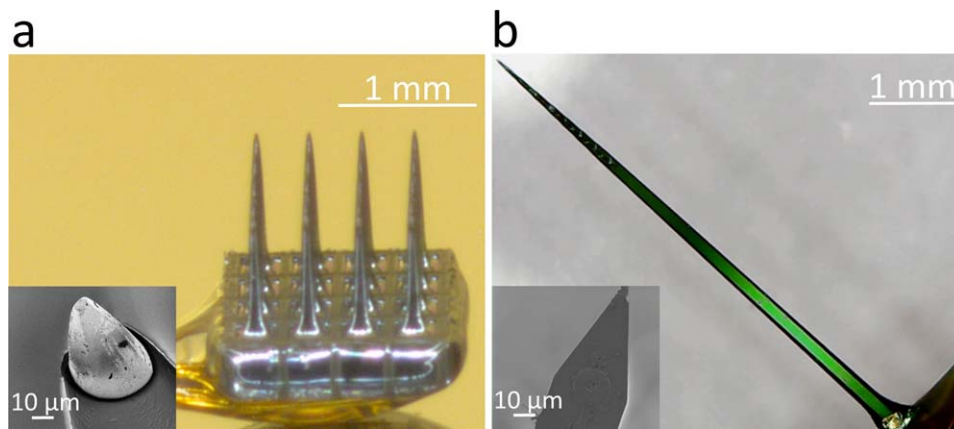


Figure 1. a. An optical micrograph of a commercial, 4 x 4 cortical microelectrode array produced by Blackrock Microsystems. Using semiconductor processing techniques, a single piece of silicon is fabricated into three dimensional, conical needles. Insulators like Parylene C provide insulation around the individual needles. The conductive tips, consisting of platinum, iridium, or iridium oxide, have a geometric surface area of approximately 2000 μm^2 ; inset shows a scanning electron micrograph of the tip. b. An optical micrograph of an A16 planar Michigan style microelectrode array produced by NeuroNexus. The array is produced in silicon substrates through the addition of multiple conductive and insulating thin films, resulting in an overall device thickness of either 15 or 50 μm . Unlike the Utah style array, the standard singular planar “shank” hosts multiple electrodes, in either linear columns, down the edge of the electrode, or arrayed in sets of four known as tetodes. The SEM inset shows that limitations from both the planar, two-dimensional surface, and real estate lost to route the electrode traces down the shaft of the implant, lead to the NeuroNexus electrodes possessing a smaller geometric surface area of approximately 176 μm^2 . [Color figure can be viewed at wileyonlinelibrary.com]

iridium oxide coating of 2000 μm^2 . The Michigan (or Neuronexus) array commonly consists of a single shank of length 3–5 mm with a thickness of 15–50 μm and multiple substrate integrated microelectrode contacts of 121–1250 μm^2 . Both of these array structures have been used for neural stimulation applications (12,13). For example, the Utah array has been used to explore restoration of tactile and proprioceptive feedback where patterned stimuli are provided as current pulses of 20–80 μA to the human sensory cortex (14). Furthermore, the Utah slant array, consisting of shanks of decreasing length to allow access to fascicular structures, has emerged as one of several strategies for peripheral nerve stimulation (15). These arrays have feature sizes an order of magnitude smaller than those of DBS electrodes and offer enhanced specificity for more precise and selective delivery of stimulation. Nevertheless, implantation of both the Utah and Michigan arrays, as well as arrays of microwires, triggers a chronic tissue response which is associated with a loss of neural cell bodies and processes proximal to the microelectrode sites (16,17). The details associated with the neuroinflammatory response have been well-documented and described previously. In short, this biotic mechanism is believed to originate from the chronic foreign body response (FBR) following initial implantation, and downstream processes that have features consistent with neurotrauma and neurodegeneration (18–23).

Evidence suggests that mechanical mismatch between an implanted device and the surrounding brain tissue plays a significant role in the tissue response. Figure 2 compares the elastic or Young’s modulus of various materials used in brain implants and surrounding tissue. Brain tissue exhibits a Young’s modulus on the order of 1–10 kPa, whereas Young’s modulus for silicon, a common implantable device material, is 130–170 GPa (27). There is a substantial literature concerning probes consisting of materials which have a relatively low degree of stiffness, that is, nearing 10–20 MPa, that appear to elicit decreased tissue response in comparison to their stiffer counterparts (34). The central argument is that soft implantable probes blunt the micromotion induced strain believed to be the source of chronic inflammation (35).

A seemingly different approach to dealing with the tissue response problem may be to reduce physical dimensions of the

device. Interestingly, the evolution of electronics can be characterized, at least in part, with the reduction in feature size of components and devices within integrated circuits (36), and the future progress of neurotechnology may also follow this path. While for electronics, “thinking small” results in improvements in circuit speed and efficiency, for implantable neural interfaces, the result may be a device that can evade the FBR. Quite recently, there have been several studies demonstrating that ultrasmall microelectrodes offer an apparent benefit with regard to the tissue response (37,38). These

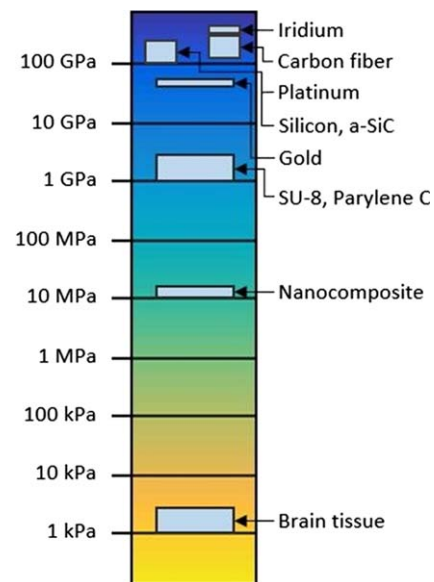


Figure 2. Log scale plot comparing Young’s modulus of commonly used implant materials. Implantable electrodes are usually fabricated from high modulus materials such as silicon, which exhibits a modulus 6–7 orders of magnitude higher than that of brain tissue. Softer, polymeric materials such as SU-8 and bio-inspired nanocomposites may decrease this gap by 3–4 orders of magnitude. Values for moduli of each substrate were taken from published literature: Iridium (24), carbon fiber (25,26), platinum (24), silicon (27), a-SiC (28), gold (29), SU-8 (30), Parylene C (31), nanocomposite (32), and human brain tissue (33). [Color figure can be viewed at wileyonlinelibrary.com]

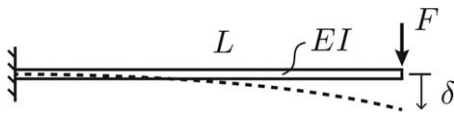


Figure 3. Cartoon depiction of the stiffness of a cantilevered beam subjected to transverse mechanical loads as a representation for a brain implant of length L . I is the moment of inertia, E is the inherent stiffness or modulus of the material, and F is the force required for a deflection, δ .

devices are fabricated of materials that inherently exhibit a high modulus of elasticity, but the small cross-sectional areas make them flexible within the brain. Small, compliant devices may decrease the volumetric displacement of brain tissue and minimize the risk of disrupting vascular structures such that there is a significant reduction or elimination of neuroinflammation. The purpose of this paper is to review our current understanding pertaining to the relationship between implant size and tissue response, the state-of-the-art in ultrasmall microelectrodes, discuss the advantages and limitations, and identify future research and development opportunities.

BIOMECHANICS OF FLEXIBLE DEVICES

Broadly speaking, stiffness (or compliance) connotes a resistance (or susceptibility) to mechanical deformation. In general, the stiffness of a mechanical structure such as a brain implant depends upon both its geometry and material composition. Stiffness can be measured experimentally by subjecting the structure to a sequence of increasing mechanical loads. The magnitudes of these loads can then be plotted with respect to some measure of deformation (e.g., elongation, deflection). For small deformations, the “stiffness” is taken to be the proportionality constant between these quantities. One can make an estimate of a brain implant’s susceptibility to bending by modeling as a cantilevered beam subjected to transverse mechanical loading (Fig. 3). The stiffness of the beam or, in our case, the implant, is a function of both the area moment of inertia of the cross-section, I , and the elastic (or Young’s) modulus of the material, E . For a given end force, F , an implant of length L will exhibit a deflection, δ . Since the area moment of inertia, I , is related to the geometry of the cross-section, compliant implants can be created using either ultrathin geometries, which reduce the moment of inertia, or extremely soft materials. Reducing cross sectional dimensions is particularly effective in increasing the compliance of an electrode since the moment of inertia is proportional to the fourth power of the device radius for a circular cross section or the third power of thickness in the bending direction for a rectangular cross section. For purposes of this review, we focus on state-of-the-art ultrasmall microelectrode arrays which achieve flexibility through small dimensions.

SILICON DEVICES WITH SMALLER CROSS-SECTIONAL AREAS REDUCE TISSUE RESPONSE

With respect to tissue response, Ratner’s group has studied and reviewed the relationship between implant size and FBR, especially for subcutaneous sensors (39,40). In general, the smaller the sensor size, the less the inflammation due to initial disruption to the surrounding tissue and sustained inflammation from the continued presence of the implant (39). Just how small does an implant need

to be to avert a tissue response? The lore among neural engineers suggests that feature sizes below $6\ \mu\text{m}$ should eliminate the tissue response. This threshold appears to be inspired by findings that the single polymer fibers with diameters below that level, implanted subcutaneously parallel to the surface of the skin, evoke little or no response (41). It was hypothesized that disruption of the extracellular matrix oriented parallel to the skin was the basis for the FBR such that thicker implants would augment the disruption and consequently increase the tissue response (39,42). Even though neural interfaces are implanted perpendicular to the surface into highly vascularized tissue, studies suggest some consistency with this sub- $10\ \mu\text{m}$ threshold. In one of relatively few studies, Seymour and Kipke examined the tissue response as a function of feature size of the implantable probe (43). The test structure consisted of a single shank containing a major architectural feature consisting of a regular rectangular lattice design, composed of structures with 4, 10, and $30\ \mu\text{m}$ side walls. Lattice dimensions below $5\ \mu\text{m}$ seem to have attenuated cell attachment to its surface, resulting in diminished astrocyte activation associated with the tissue response and concomitant retention of neurons proximal to the sites. In addition, Stice et al. compared the tissue response evoked by 12 and $25\ \mu\text{m}$ diameter thin microelectrodes showing statistically significant reductions, although not elimination, in activated astrocyte staining for smaller diameter probes after 4 weeks implantation (44). Stice et al. suggested three possible reasons for this attenuated tissue response: 1) less CNS tissue displacement with smaller dimension probes; 2) less surface area for adhesion of cells necessary to trigger inflammatory processes; 3) enhanced flexibility of probes with smaller cross-sectional areas. Another possibility put forth by Skousen et al. is that the FBR is due to the persistence of activated macrophages and subsequent release of neurotoxic biomolecules; the larger surface area causes concentration elevations proximal to the biotic–abiotic interface (45). It is noteworthy that relatively large implants that become flexible by softening within the brain also show decreased tissue response (34). While both mechanical and geometric factors are important to the tissue response (46), there appears to be a geometric threshold at or below $\sim 10\ \mu\text{m}$ diameter or a cross-sectional area of under $\sim 100\ \mu\text{m}^2$.

While it may seem straightforward to simply create thinner silicon structures as neural implants, material limitations become evident at small scales. Silicon is brittle, will dissolve over time *in vivo*, and for 1.5–2 mm long probes of thickness of $15\ \mu\text{m}$, buckling of the probe during insertion and fracture can occur (47). It is also important to recognize that with a reduction in the size of an implant, the microelectrode sites themselves become smaller posing significant challenges at the electrode–electrolyte interface.

ELECTRICAL INTERFACE CHALLENGES FOR SMALL MICROELECTRODES

Neural stimulation and recording works by a remarkable electrochemical reaction which occurs at the electrode–electrolyte interface. Electrical devices including amplifiers and stimulators operate with the flow of electrons but, physiologically, charge movement is carried by hydrated anions and cations. Conversion occurs at the electrode–electrolyte interface where the larger the surface area of an electrode, the more readily the conversion between electronic and ionic charge can proceed. Decreasing the surface area of any electrode raises the measured impedance of the electrode–electrolyte interface, thereby increasing the thermal, or Johnson, noise, and compromising the ability to transfer electrical charge

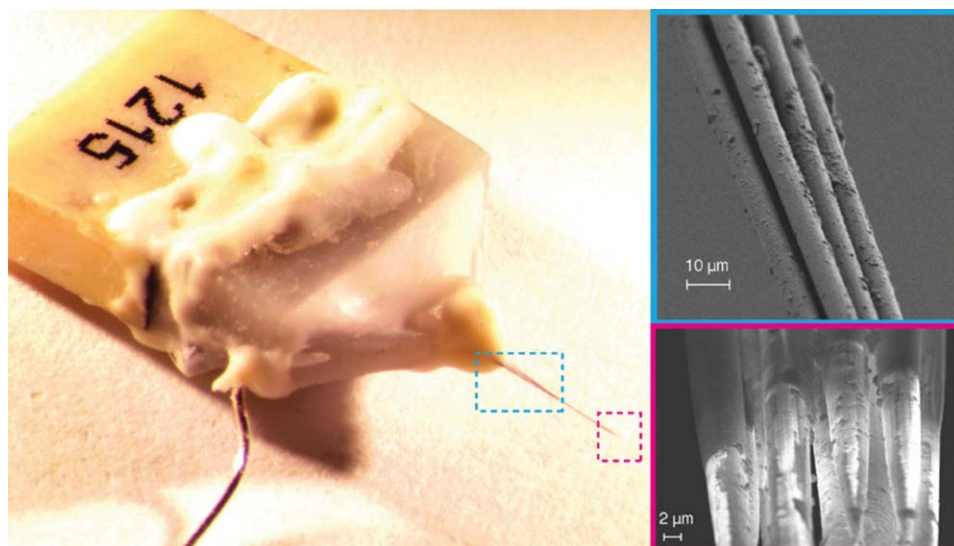


Figure 4. Bundled 16-channel carbon fiber electrode array. When drawn from water bath, the individual shanks are held by weak van der Waals attraction forming an electrode bundle about 26 μm in diameter (upper right). The fire-sharpened process de-insulates the Parylene C coatings creating an exposed electrode tip whose geometric surface area depends largely on the length of the de-insulated fiber (bottom right). From Guitchounts et al. (26) with permission. [Color figure can be viewed at wileyonlinelibrary.com]

between the electrode and the tissue. Thermal noise at an electrode–electrolyte interface is proportional to the square root of the real component of the impedance, large impedances make it difficult to separate small extracellular signals from baseline noise. For electrical stimulation, it is important to avoid faradaic reactions that may result in nonreversible, toxic interactions with the surrounding tissue (48). In addition, current injection should produce potentials at the electrode that fall within the “water window.” Exceeding these thresholds, which depend on the particular electrode material, will trigger the electrolysis of water to liberate oxygen; alternatively, if the voltage falls below a negative threshold, hydrogen is produced. Clearly, these irreversible reactions are deleterious to the electrode and surrounding tissue. The amount of charge that can be reversibly injected during a stimulation pulse while the potential remains within the water window is called the charge injection capacity, a parameter that is related to the electrode material and the surface area. When microelectrode sites become too small, they may not provide a sufficient level of charge per stimulation phase to evoke neural activity (49). For example, gold microelectrodes with a surface area of only 100 μm^2 have a charge injection capacity below 0.067 mC/cm^2 . If at least 1–2 nC/phase for a 200 μsec pulse is required to trigger cortical excitation (11,50), then such small microelectrodes fall short. Instead, a charge injection capacity of at least 1–2 mC/cm^2 is necessary for effective neural stimulation with microelectrode of this size.

So how do we achieve low impedance and high charge capacity for a small microelectrode? The answer: by coating microelectrode sites with materials that increase reduction-oxygen capacity and effective electrochemical surface area. There are a number of approaches for coating microelectrodes with ceramics, conductive polymers, or metallic oxides. Nonpolymeric approaches include sputtered iridium oxide (SIROF), titanium nitride (TiN) (51), or electrodeposited iridium oxide (EIROF) (52) which provide high charge injection capacity and low impedance coatings for electrodes. For example, sputtered iridium oxide can produce a maximum charge injection capacity between 1 and 5 mC/cm^2 , which is 10–100 times

greater than Pt or Pt/Ir (11). With respect to conductive polymers, the most commonly used coating strategy is poly(3,4-ethylenedioxythiophene) or PEDOT, which is often deposited through oxidative polymerization of ethylenedioxythiophene in the presence of poly(styrenesulfonate) or PSS onto microelectrode sites (53). Cui and Martin demonstrated that application of PEDOT-PSS to microelectrodes decreased the impedance by almost two orders of magnitude (54). PEDOT-PSS also displayed a 15-fold improvement in charge-injection capacity of $\sim 15 \text{ mC}/\text{cm}^2$ (55). The problem for PEDOT-PSS is durability, and while electrodeposition of PEDOT with a tetrafluoroborate (56,57) or perhaps inclusion of appropriately functionalized carbon nanotubes (58) improves electrochemical performance and stability, long term robustness especially for neural stimulation remains elusive. Instead, metallic/oxide-based coatings are more likely to demonstrate long term stability *in vivo* for neural stimulation applications. Recently, ultrasmall microelectrodes have emerged that leverage conductive materials such as carbon that enable small size for minimizing tissue response.

ULTRASMALL CARBON-FIBER BUNDLES FOR NEUROSTIMULATION AND RECORDING

The use of carbon fiber electrodes for the voltammetric/ amperometric detection and quantification of neurochemicals such as dopamine is well known (59,60). For neural recording or stimulation, carbon fibers are electrically conductive and their small cross-sectional area makes them attractive due to their minimal invasiveness during implantation, minimal risk of blood-brain-barrier disruption, and reduced tissue displacement (37,61,62). Carbon fibers have a typical radii of about 4–7 μm and are mechanically stiff with a Young’s modulus of 241–380 GPa (25,26). The small cross-sectional area allows the fibers to be mechanically compliant within neuronal tissues (62). Implanted carbon fiber microelectrodes have provided high quality single and multiunit recordings in acute and chronic experiments (25,26,62). Carbon fiber microelectrodes have been shown to record at high signal-to-noise from a variety of neuronal

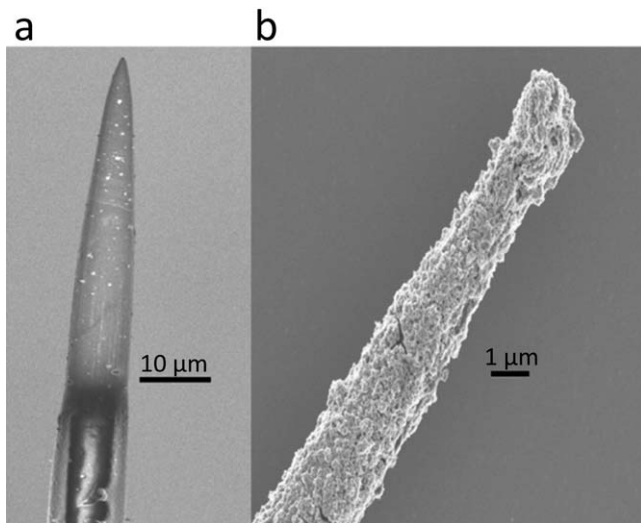


Figure 5. Scanning electron micrograph of a fire-sharpened carbon fiber electrode tip before (a) and after (b) electrodeposited iridium oxide film (EIROF) coatings. EIROF coatings improved the electrochemical properties of the electrode. The nodular surface morphology of EIROF creates a higher electrochemical surface area for charge transfer. With appropriate positive biasing, EIROF coated carbon fiber can readily injected 4 nC/ph in a 200 μ sec and 400 μ sec pulses without exceeding water electrolysis limits.

cell types, across a variety of brain regions at varying depth in different animal models including songbirds (26) and rat cortex (25,62). As shown in Figure 4, carbon fibers, inserted as bundles that agglomerate when wet to allow insertion without buckling, appear to splay within the tissue to behave as 3D arrays that sample from a volume of neural tissue (26). Splaying dynamics, however, may rely on a delicate balance between the Van der Waal's force that induces bundling and the tissue mechanics. While penetration and splaying occurs in songbird cortex with carbon fiber bundles, it may or may not work reliably in other species of brain structures that have differing mechanical characteristics.

There are three major disadvantages of carbon fiber microelectrodes that limit widespread use for neural stimulation applications: 1) The electrochemical characteristics of bare carbon in physiological saline are poorly suited for neural recording and stimulation. For an exposed geometric surface area of 500 μm^2 , carbon fibers show impedance levels of greater than 1 M Ω at 1 kHz and a charge-injection limit below 0.05 mC/cm². The majority of prior work with carbon fiber tips has relied on coatings with PEDOT-PSS or PEDOT-PSS with carbon nanotubes (58). Unfortunately, as previously noted, PEDOT is unlikely to provide a stable electrochemical interface for chronic neural stimulation. An alternative to PEDOT is coating with EIROF, which have been demonstrated to create stable interfaces for neural stimulation (52,63,64). Coating the tips of carbon fibers with EIROF produced a highly nodular electrode surface (Fig. 5) which reduced the electrode impedance by 10-fold and increased the charge injection capacity to 17 mC/cm² with appropriate biasing. 2) Regardless of coatings, the fiber-based microelectrodes are fabricated by hand. The tips of carbon fibers, which are coated with a thin layer of Parylene C for insulation, are opened at the distal end either mechanically by using surgical scissors or razor blade to expose the active microelectrode site or by thermal ablation usually with a flame (26). Manual fabrication limits the ability to create reproducible structures for wide spread use and commercial dissemination.

FUTURE OPPORTUNITIES FOR REPRODUCIBLE AND SCALABLE FABRICATION OF ULTRASMALL MICROELECTRODE ARRAYS

The key to creating reproducible microscale devices is by leveraging state-of-the-art photolithography and microfabrication techniques. Very recently, Luan et al. reported the development and demonstration of ultrathin linear arrays of microelectrodes (38). Composed of SU-8, which is conventionally used in microfabrication laboratories as a photo-resist, two types of multilayer probes have been described that are 1 μm in thickness and possess microelectrode widths of either 10 or 50 μm . With such small cross-sectional areas, these highly flexible devices exhibit little or no tissue response after months of implantation in mice where single unit neuronal activity could be readily resolved. While the electrode sites are either Pt or Au, coatings including EIROF or SIROF would likely enable microscale neural stimulation applications. While SU-8 has a relatively positive literature supporting its *in vitro* and *in vivo* biocompatibility (65), it is not typically found in implantable biomedical devices and providers (e.g., MicroChem) may be hesitant to grant use for medical applications. Nevertheless, we remain optimistic that polymers, including those with shape memory thermomechanical characteristics (66,67), offer a solution for implantable microscale devices. We note that polymeric materials including silicone, parylene, and polyamide, are all components of the Medtronic DBS Lead Model 3387.

Alternatively, amorphous silicon carbide (a-SiC) has emerged as a candidate encapsulation material for next generation brain implants (68–71). Created through plasma enhanced chemical vapor deposition, a-SiC films exhibit robust long-term stability, high electronic resistivity, and resistance to corrosion (68,72,73). Moreover, a-SiC has an established track record as a biomedical device material, specifically as a coronary stent coating (74). Prototype arrays of microelectrodes designed for intracortical stimulation and recording that utilize a-SiC as a structural and insulating material have been developed by the Cogan group and are shown in Figure 6. These devices consist of individual shanks <10 μm wide yielding a shank cross-sectional area of <60 μm^2 . These small dimensions and mechanical robustness of the film enable overall device flexibility. In contrast to carbon fibers, a-SiC processing is amenable to thin-film fabrication processes and photolithography. In addition, a-SiC devices can be readily customized and reliably reproduced at scales necessary for translation. To achieve suitable charge injection capacity, microelectrode sites can be coated with SIROF or porous TiN to produce low impedance coatings resulting in 100 μm^2 sites with charge injection capacities >3 mC/cm². These devices have the potential to achieve highly spatially selective neural stimulation under chronic conditions where the tissue response is minimized due to the small physical dimensions.

PRACTICAL CONSIDERATIONS FOR CLINICAL USE OF ARRAYS OF ULTRASMALL MICROELECTRODES

After fabrication issues are solved, there will be a challenge with respect to *in vivo* imaging of the ultrasmall microelectrodes to verify the exact position in the brain after implantation. The value of spatial resolution enabled by ultrasmall microelectrodes will be limited if devices are readily dislodged or experience migration. Experiments in rodents with 7T magnetic resonance imaging (MRI) demonstrated

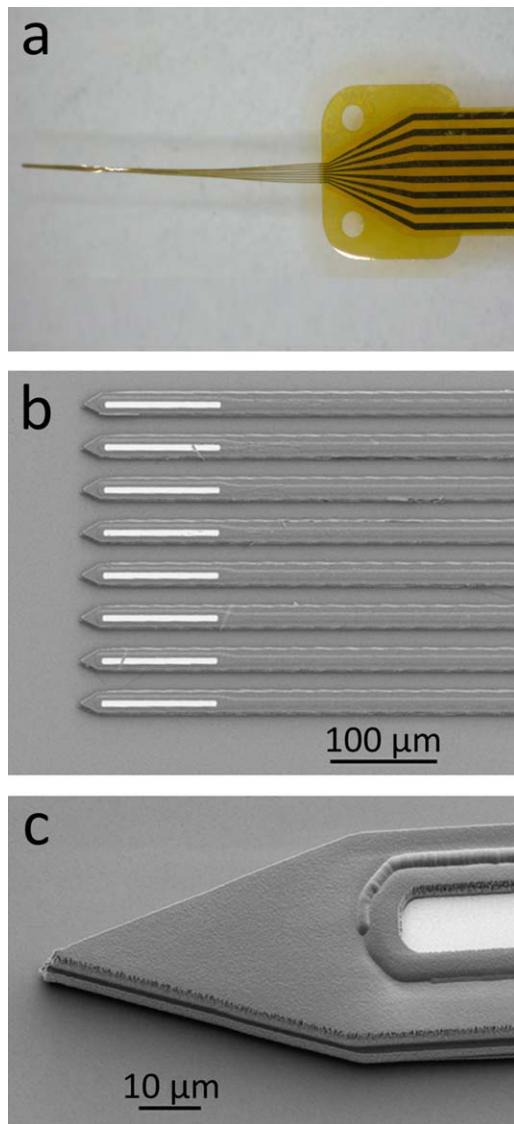


Figure 6. An 8-channel a-SiC microelectrode array (MEA) developed using standard semiconductor fabrication processes. The MEAs are fabricated on a thin layer of polyimide which is spin-coated on a silicon carrier wafer. After fabrication, the carrier wafer is soaked in deionized water to release the devices. a. When withdrawn from deionized water, the shanks of the a-SiC MEA forms a bundle. b. optical micrograph showing the electrode sites at the distal end of the array. Electrode openings are created by reactive ion etching. c. scanning electron micrograph showing the tip profile with a near-vertical sidewall created using an inductively coupled plasma etching system. [Color figure can be viewed at wileyonlinelibrary.com]

imaging of 50 µm diameter Tungsten microwires (75,76), however the limited resolution of clinical MRI will be problematic for imaging ultrasmall microelectrodes. Furthermore, a consequence of microscale neural stimulation strategies will likely be the challenge of programming a larger number of electrode sites. For DBS, programming is typically performed empirically by surveying the effects of monopolar stimulation to determine an optimal stimulation configuration. It may not be practical to survey the vast parameter space associated with potentially many ultrasmall microelectrodes. Model based optimization approaches may facilitate discovery of optimal settings (77), but it is also entirely likely that there will be only marginal improvement in therapy for certain disorders treated with DBS given the volume of tissue required for activation to achieve results

(78). Instead, the benefits of spatial precision enabled by microscale neural stimulation are more likely to be realized for emergent neuroprosthetic applications such as restoration of proprioceptive/tactile sensation or visual perception through cortical stimulation. In these applications, the topographic organization of the brain cortices and relationship to sensation will aid in the initial programming stage, however the large neurostimulation parameter space will remain a challenge.

CONCLUSION

A natural evolution for electronic devices, including those of biomedical use, involves the decrease in size. For chronically implantable neural interfaces, “thinking small” results in size scales approaching the dimensions of cells within the brain, offering the possibility of more selective spatial stimulation and minimization of the tissue reactions by effectively evading the FBR. This tissue response likely involves both the inherent stiffness of the materials comprising the device and the physical dimensions of the implant. Extremely flexible devices of sufficiently small cross-sectional areas can be fabricated from inherently stiff and physically robust materials. For any ultrasmall microelectrode technology to become reproducible and ultimately translatable to the clinic, it is vital that devices can be created at scale and are comprised of robust materials. In spite of its widespread use, Parylene C is well known to have significant limitations with respect to robustness (79) necessitating the exploration of alternative materials such as liquid crystal polymers, which are chemically inert and have very low permeability (80). Alternatively, a-SiC has advantages as an extremely robust structural and insulating material that can be coupled with state-of-the-art microelectrode coatings such as SIROF to enable a wide range of microscale neural stimulation applications. Future studies will be necessary to compare the relative merits of probes of differing materials including a-SiC with respect to tissue response and device longevity. Testing under *in vivo* conditions is particularly important, since the rigors of *in vivo* stimulation can stress thin-film devices and could lead to dissolution of metal contact pads or their coatings, as well as other modes of device failure such as delamination.

Authorship Statements

Drs. Joseph Pancrazio and Stuart Cogan organized and interpreted the core ideas and contributed the main text of the manuscript. Dr. Victor Varner contributed significant concepts on biomechanics of implantable probes. Felix Deku and Dr. Timothy Gardner contributed ideas on amorphous silicon carbide-based implantable devices and carbon fiber-based devices. Atefeh Ghazavi and Rashed Rihani provided a survey of electrical properties of novel coatings. Allison M. Stiller contributed a survey of material properties associated with implantable devices. Dr. Christopher L. Frewin contributed ideas associated with the tissue response to implantable devices.

How to Cite this Article:

Pancrazio J.J., Deku F., Ghazavi A., Stiller A.M., Rihani R., Frewin C.L., Varner V.D., Gardner T.J., Cogan S.F. 2017. Thinking Small: Progress on Microscale Neurostimulation Technology. *Neuromodulation* 2017; 20: 745–752

REFERENCES

1. Benabid AL, Pollak P, Gao DM et al. Chronic electrical stimulation of the ventralis intermedius nucleus of the thalamus as a treatment of movement disorders. *J Neurosurg* 1996;84:203–214.
2. Flora ED, Perera CL, Cameron AL, Maddern GJ. Deep brain stimulation for essential tremor: a systematic review. *Mov Disord* 2010;25:1550–1559.
3. Perlmutter JS, Mink JW. Deep brain stimulation. *Annu Rev Neurosci* 2006;29:229–257.
4. Wichmann T, DeLong MR. Deep brain stimulation for neurologic and neuropsychiatric disorders. *Neuron* 2006;52:197–204.
5. Abelson JL, Curtis GC, Sagher O et al. Deep brain stimulation for refractory obsessive-compulsive disorder. *Biol Psychiatry* 2005;57:510–516.
6. Mayberg HS, Lozano AM, Voon V et al. Deep brain stimulation for treatment-resistant depression. *Neuron* 2005;45:651–660.
7. Servello D, Porta M, Sassi M, Brambilla A, Robertson MM. Deep brain stimulation in 18 patients with severe Gilles de la Tourette syndrome refractory to treatment: the surgery and stimulation. *J Neurol Neurosurg Psychiatry* 2008;79:136–142.
8. Butson CR, Moks CB, McIntyre CC. Sources and effects of electrode impedance during deep brain stimulation. *Clin Neurophysiol* 2005;117:447–454.
9. Contarino MF, Bour LJ, Verhagen R et al. Directional steering: a novel approach to deep brain stimulation. *Neurology* 2014;83:1163–1169.
10. Steigerwald F, Müller L, Johannes S, Matthies C, Volkmann J. Directional deep brain stimulation of the subthalamic nucleus: a pilot study using a novel neurostimulation device. *Mov Disord* 2016;31:1240–1243.
11. Cogan SF. Neural stimulation and recording electrodes. *Annu Rev Biomed Eng* 2008;10:275–309.
12. Torab K, Davis TS, Warren DJ, House PA, Normann RA, Greger B. Multiple factors may influence the performance of a visual prosthesis based on intracortical microstimulation: nonhuman primate behavioural experimentation. *J Neural Eng* 2011;8:035001.
13. Frost SB, Dunham CL, Barbay S et al. Output properties of the cortical hindlimb motor area in spinal cord-injured rats. *J Neurotrauma* 2015;32:1666–1673.
14. Flesher SN, Collinger JL, Folds ST et al. Intracortical microstimulation of human somatosensory cortex. *Sci Transl Med* 2016;8:361ra141.
15. Davis TS, Wark HAC, Hutchinson DT et al. Restoring motor control and sensory feedback in people with upper extremity amputations using arrays of 96 microelectrodes implanted in the median and ulnar nerves. *J Neural Eng* 2016;13:036001.
16. Ward MP, Rajdev P, Ellison C, Irazoqui PP. Toward a comparison of microelectrodes for acute and chronic recordings. *Brain Res* 2009;1282:183–200.
17. Jorfi M, Skousen JL, Weder C, Capadona JR. Progress towards biocompatible intracortical microelectrodes for neural interfacing applications. *J Neural Eng* 2015;12:011001.
18. Rousche PJ, Normann RA. Chronic recording capability of the Utah intracortical electrode array in cat sensory cortex. *J Neurosci Meth* 1998;82:1–15.
19. Turner JN, Shain W, Szarowski DH et al. (1999) Cerebral astrocyte response to micro-machined silicon implants. *Exp Neurol* 1999;156:33–49.
20. Szarowski DH, Andersen MD, Retterer S et al. Brain responses to micro-machined silicon devices. *Brain Res* 2003;983:23–35.
21. Biran R, Martin DC, Tresco PA. Neuronal cell loss accompanies the brain tissue response to chronically implanted silicon microelectrode arrays. *Exp Neurol* 2005;195:115–126.
22. Polikov VS, Tresco PA, Reichert WM. Response of brain tissue to chronically implanted neural electrodes. *J Neurosci Methods* 2005;148:1–18.
23. Grill WM, Norman SE, Bellamkonda RV. Implanted neural interfaces: biochallenges and engineered solutions. *Annu Rev Biomed Eng* 2009;11:1–24.
24. Merker J, Lupton D, Töpfer M, Knake H. High temperature mechanical properties of the platinum group metals. *Platinum Metals Rev* 2001;45:74–82.
25. Patel PR, Na K, Zhang H et al. Insertion of linear 8.4 μm diameter 16 channel carbon fiber electrode arrays for single unit recordings. *J Neural Eng* 2015;12:046009.
26. Guitchounts G, Markowitz JE, Liberti WA, Gardner TJ. A carbon-fiber electrode array for long-term neural recording. *J Neural Eng* 2013;10:046016.
27. Cho CH. Characterization of Young's modulus of silicon versus temperature using a "beam deflection" method with a four-point bending fixture. *Curr Appl Physics* 2009;9:538–545.
28. Kulikovskiy V, Vorlíček V, Boháč P et al. Hardness and elastic modulus of amorphous and nanocrystalline SiC and Si films. *Surf Coat Technol* 2008;202:1738–1745.
29. Salvadori MC, Brown IG, Vaz AR, Melo LL, Cattani M. Measurement of the elastic modulus of nanostructured gold and platinum thin films. *Phys Rev B* 2003;67:153404.
30. Lorenz H, Despont M, Fahrni N, LaBianca N, Renaud P, Vettiger P. SU-8: a low-cost negative resist for MEMS. *J Micromech Microeng* 1997;7:121.
31. Hassler C, von Metzner RP, Ruther P, Stieglitz T. Characterization of parylene C as an encapsulation material for implanted neural prostheses. *J Biomed Mater Res B Appl Biomater* 2010;93:266–274.
32. Shanmuganathan K, Capadona JR, Rowan SJ, Weder C. Stimuli-responsive mechanically adaptive polymer nanocomposites. *ACS Appl Mater Interfaces* 2010;2:165–174.
33. Budday S, Nay R, de Rooij R et al. Mechanical properties of gray and white matter brain tissue by indentation. *J Mech Behav Biomed Mater* 2015;46:318–330.
34. Nguyen JK, Park DJ, Skousen JL et al. Mechanically-compliant intracortical implants reduce the neuroinflammatory response. *J Neural Eng* 2014;11:056014.
35. Sridharan A, Nguyen JK, Capadona JR, Muthuswamy J. Compliant intracortical implants reduce strains and strain rates in brain tissue in vivo. *J Neural Eng* 2015;12:036002.
36. Rizal B, Merlo JM, Burns MJ, Chiles TC, Naughton MJ. Nanocoaxes for optical and electronic devices. *Analyst* 2015;140:39–58.
37. Kozai TD, Marzullo TC, Hooi F et al. Reduction of neurovascular damage resulting from microelectrode insertion into the cerebral cortex using in vivo two-photon mapping. *J Neural Eng* 2010;7:046011.
38. Luan L, Wei X, Zhao Z et al. Ultraflexible nanoelectronic probes form reliable, glial scar-free neural integration. *Sci Adv* 2017;3:e1601966.
39. Helton KL, Ratner BD, Wisniewski NA. Biomechanics of the sensor-tissue interface-effects of motion, pressure, and design on sensor performance and the foreign body response-part I: theoretical framework. *J Diabetes Sci Technol* 2011;5:632–646.
40. Helton KL, Ratner BD, Wisniewski NA. Biomechanics of the sensor-tissue interface-effects of motion, pressure, and design on sensor performance and foreign body response-part II: examples and application. *J Diabetes Sci Technol* 2011;5:647–656.
41. Sanders JE, Stiles CE, Hayes CL. Tissue response to single-polymer fibers of varying diameters: evaluation of fibrous encapsulation and macrophage density. *J Biomed Mater Res* 2000;52:231–237.
42. Sanders JE, Cassisi DV, Neumann T et al. Relative influence of polymer fiber diameter and surface charge on fibrous capsule thickness and vessel density for single-fiber implants. *J Biomed Mater Res A* 2003;65:462–467.
43. Seymour JP, Kipke DR. Neural probe design for reduced tissue encapsulation in CNS. *Biomaterials* 2007;28:3594–3607.
44. Stice P, Gilletti A, Panitch A, Muthuswamy J. Thin microelectrodes reduce GFAP expression in the implant site in rodent somatosensory cortex. *J Neural Eng* 2007;4:42–53.
45. Skousen JL, Merriam SM, Srivannavit O, Perlin G, Wise KD, Tresco PA. Reducing surface area while maintaining implant penetrating profile lowers the brain foreign body response to chronically implanted planar silicon microelectrode arrays. *Prog Brain Res* 2011;194:167–180.
46. Spencer KC, Sy JC, Ramadi KB, Graybiel AM, Langer R, Cima MJ. Characterization of mechanically matched hydrogel coatings to improve the biocompatibility of neural implants. *Sci Rep* 2017;7:1952.
47. Weltman A, Yoo J, Meng E. (2016) Flexible, penetrating brain probes enabled by advances in polymer microfabrication. *Micromachines* 2016;7:180.
48. Merrill DR, Bikson M, Jefferys JG. Electrical stimulation of excitable tissue: design of efficacious and safe protocols. *J Neurosci Meth* 2005;141:171–198.
49. Cogan SF, Ehrlich J, Plante TD et al. Sputtered iridium oxide films for neural stimulation electrodes. *J Biomed Mater Res B Appl Biomater* 2009;89:353–361.
50. McCreery DB. Cochlear nucleus auditory prostheses. *Hear Res* 2008;242:64–73.
51. Weiland JD, Anderson DJ, Humayun MS. In vitro electrical properties for iridium oxide versus titanium nitride stimulating electrodes. *IEEE Trans Biomed Eng* 2002;49:1574–1579.
52. Meyer RD, Cogan SF, Nguyen TH, Rauh RD. Electrodeposited iridium oxide for neural stimulation and recording electrodes. *IEEE Trans Neural Syst Rehabil Eng* 2001;9:2–11.
53. Forcelli PA, Sweeney CT, Kammerich AD et al. Histocompatibility and in vivo signal throughput for PEDOT, PEDOP, P3MT, and polycarbazole electrodes. *J Biomed Mater Res A* 2012;100:3455–3462.
54. Cui X, Martin DC. Electrochemical deposition and characterization of poly(3,4-ethylenedioxythiophene) on neural microelectrode arrays. *Sens Actuators B Chem* 2003;89:92–102.
55. Venkatraman S, Hendricks J, King ZA et al. In vitro and in vivo evaluation of PEDOT microelectrodes for neural stimulation and recording. *IEEE Trans Neural Syst Rehabil Eng* 2011;19:307–316.
56. Mandal HS, Kasteel JS, McHail DG, Rubinson JF, Pancrazio JJ, Dumas TC. Improved poly(3,4-ethylenedioxythiophene) (PEDOT) for neural stimulation. *Neuromodulation* 2015;18:657–663.
57. Mandal HS, Knaack GL, Charkhar H et al. Improving the performance of poly(3,4-ethylenedioxythiophene) for brain-machine interface applications. *Acta Biomater* 2014;10:2446–2454.
58. Kozai TD, Catt K, Du Z et al. Chronic in vivo evaluation of PEDOT/CNT for stable neural recordings. *IEEE Trans Biomed Eng* 2016;63:111–119.
59. Zhang DA, Rand E, Marsh M et al. Carbon nanofiber electrode for neurochemical monitoring. *Mol Neurobiol* 2013;48:380–385.
60. Rodeberg NT, Sandberg SG, Johnson JA, Phillips PE, Wightman RM. Hitchhiker's guide to voltammetry: acute and chronic electrodes for in vivo fast-scan cyclic voltammetry. *ACS Chem Neurosci* 2017;8:221–234.
61. Bjornsson CS, Oh SJ, Al-Kofahi YA et al. Effects of insertion conditions on tissue strain and vascular damage during neuroprosthetic device insertion. *J Neural Eng* 2006;3:196–207.
62. Kozai TDY, Langhals NB, Patel PR et al. Ultrasmall implantable composite microelectrodes with bioactive surfaces for chronic neural interfaces. *Nat Mater* 2012;11:1065–1073.
63. Liu X, McCreery DB, Bullara LA, Agnew WF. Evaluation of the stability of intracortical microelectrode arrays. *IEEE Trans Neural Syst Rehabil Eng* 2006;14:91–100.
64. Han M, Manoochitwongsa PS, Wang CX, McCreery DB. In vivo validation of custom-designed silicon-based microelectrode arrays for long-term neural recording and stimulation. *IEEE Trans Biomed Eng* 2012;59:346–354.
65. Nemani KV, Moodie KL, Brennick JB, Su A, Gimi B. In vitro and in vivo evaluation of SU-8 biocompatibility. *Mater Sci Eng C Mater Biol Appl* 2013;33:4453–4459.
66. Ware T, Simon D, Liu C et al. Thiol-ene/Acrylate substrates for softening intracortical electrodes. *J Biomed Mater Res B Appl Biomater* 2014;102:1–11.
67. Simon DM, Charkhar H, St John C et al. Design and demonstration of an intracortical probe technology with tunable modulus. *J Biomed Mater Res A* 2017;105:159–168.

68. Cogan SF, Edell DJ, Guzelian AA, Ping Liu Y, Edell R. Plasma-enhanced chemical vapor deposited silicon carbide as an implantable dielectric coating. *J Biomed Mater Res A* 2003;67:856–867.
69. Hsu JM, Tathireddy P, Rieth L, Normann AR, Solzbacher F. Characterization of a-SiC(x):H thin films as an encapsulation material for integrated silicon based neural interface devices. *Thin Solid Films* 2007;516:34–41.
70. Knaack GL, McHail DG, Borda G et al. In vivo characterization of amorphous silicon carbide as a biomaterial for chronic neural interfaces. *Front Neurosci* 2016;10:301.
71. Lei X, Kane S, Cogan S et al. SiC protective coating for photovoltaic retinal prosthesis. *J Neural Eng* 2016;13:046016.
72. Azevedo RG, Zhang J, Jones DG et al. Silicon carbide coated MEMS strain sensor for harsh environment applications. In: *IEEE 20th International Conference on Micro Electro Mechanical Systems (MEMS); Kobe, Japan. 2007;643–646.*
73. Zorman CA. Silicon carbide as a material for biomedical microsystems. In: *MEMS/MOEMS, Symposium on Design, Test, Integration & Packaging of MEMS/MOEMS; Rome, Italy. 2009;1–7.*
74. Kalnins U, Erglis A, Dinne I, Kumsars I, Jegere S. Clinical outcomes of silicon carbide coated stents in patients with coronary artery disease. *Med Sci Monit* 2002;8:P116–P120.
75. Neuberger T, Paralikar K, Zhang Z, Clement RS, Webb A. Monitoring brain dimpling and intracortical micro-electrode arrays with high resolution MRI in rats. *Proc Intl Soc Mag Reson Med* 2007;15:2352.
76. Paralikar KJ, Neuberger T, Matsui JT, Barber AJ, Webb A, Clement RS. (2009) Feasibility and safety of longitudinal magnetic resonance imaging in a rodent model with intracortical microwire implants. *J Neural Eng* 2009;6:034001.
77. Xiao Y, Peña E, Johnson MD. Theoretical optimization of stimulation strategies for a directionally segmented deep brain stimulation electrode array. *IEEE Trans Biomed Eng* 2016;63:359–371.
78. Teplitzky BA, Zitella LM, Xiao Y, Johnson MD. Model-based comparison of deep brain stimulation array functionality with varying number of radial electrodes and machine learning feature sets. *Front Comput Neurosci* 2016;10:58.
79. Minnikanti S, Diao G, Pancrazio JJ et al. Lifetime assessment of atomic-layer-deposited Al₂O₃-Parylene C bilayer coating for neural interfaces using accelerated age testing and electrochemical characterization. *Acta Biomater* 2014;10:960–967.
80. Fekete Z, Pongrácz A. Multifunctional soft implants to monitor and control neural activity in the central and peripheral nervous system: a review. *Sens Actuators B Chem* 2017;243:1214–1223.